Hindawi Publishing Corporation
Journal of Nanomaterials
Volume 2016, Article ID 7818501, 13 pages
http://dx.doi.org/10.1155/2016/7818501

Research Article

Functionalized Solid-Sphere PEG-*b*-PCL Nanoparticles to Target Brain Capillary Endothelial Cells *In Vitro*

Philip Grossen,[1] Gabriela Québatte,[1] Dominik Witzigmann,[1] Cristina Prescianotto-Baschong,[2] Le-Ha Dieu,[1] and Jörg Huwyler[1]

[1]*Division of Pharmaceutical Technology, Department of Pharmaceutical Sciences, University of Basel, 4056 Basel, Switzerland*
[2]*Biozentrum University of Basel, 4056 Basel, Switzerland*

Correspondence should be addressed to Jörg Huwyler; joerg.huwyler@unibas.ch

Received 23 February 2016; Revised 4 May 2016; Accepted 12 May 2016

Academic Editor: Jean M. Greneche

Nanoparticles are increasingly used to implement drug targeting strategies. In the present study, solid-sphere nanoparticles (SNPs) made of poly(ethylene glycol)-*b*-poly(ε-caprolactone) (PEG-*b*-PCL) were covalently linked to a monoclonal antibody (83-14 mAb) targeted against the human insulin receptor that is highly expressed on human brain microvascular endothelial cells. Resulting targeted SNPs were characterized using transmission electron microscopy (TEM), cryo-TEM, dynamic light scattering, and fluorescence correlation spectroscopy. The critical aggregation concentration was determined using a fluorescence approach. Interaction with a well-characterized human *in vitro* model of the blood-brain barrier (hCMEC/D3) was analysed using an array of methods (flow cytometry, confocal laser scanning microscopy, and TEM). The toxicity on hCMEC/D3 cells and in addition on the human liver cell line HepG2 was assessed using the MTT assay. SNPs with a diameter of 80 nm and a homogeneous size distribution were obtained. Successful conjugation of 83-14 mAb using a heterobifunctional linker resulted in 5-6 molecules of fluorescently labeled 83-14 mAb per SNP. Functionalized SNPs were taken up by hCMEC/D3 cells efficiently without showing a significant toxic effect on cells of the blood-brain barrier and HepG2 cells. These results indicate that functionalized PEG-*b*-PCL SNPs are a promising candidate to deliver drugs to the CNS.

1. Introduction

Despite the presence of potent active pharmaceutical ingredients (API), efficient treatment of central nervous system- (CNS-) related diseases remains a major challenge in pharmacotherapy. The blood-brain barrier (BBB) that maintains the homeostasis of the brain excludes many small and large molecule drugs from the CNS [1, 2]. To reach therapeutic concentrations of systemic administered drugs in the CNS, high doses are often required. This is linked with an increased risk for toxic side effects. Therefore, different strategies for effective drug transfer across the BBB are currently under investigation [3]. Besides chemical optimization of the API and invasive delivery techniques, targeting of transporters and receptors expressed on BBB endothelial cells is a promising way to specifically deliver drugs to the CNS [3]. Endogenous macromolecules can cross the BBB by receptor-mediated transport and thus reach the brain despite their size as shown for insulin [4, 5] and transferrin [6]. Antibodies can mimic these endogenous ligands and transport bound drugs, macromolecules, or nanoparticles across the BBB *in vivo*. For example, the enzyme N-sulfoglucosamine sulfohydrolase (SGSH) was conjugated to a monoclonal antibody (mAb) directed against the human insulin receptor (HIR). Recombinant SGSH was not able to cross the BBB. However, it was possible to reach therapeutic concentrations in the brain after injection of the mAb fusion protein in Rhesus monkeys [7]. While antibody drug conjugates (ADCs) provide specific targeting to a distinctive tissue or cell type, their drug carrying capacity is very limited. Nanocarriers can exceed the drug payload of ADCs by three to four orders of magnitude [8]. Within these nanocarriers, self-assembled micelles consisting of biodegradable diblock copolymers are extensively studied as drug delivery systems (DDS) [9]. Their hydrophobic core serves as a reservoir for poorly soluble drugs, sterically stabilized by a hydrophilic corona [10]. Polymeric micelles

can prevent premature drug degradation, reduce off-target effects, and increase bioavailability. In addition, these systems can be directed towards specific organs, tissues, or cells by coupling targeting moieties onto their surface [11]. In recent years, various approaches were investigated to combine NPs with BBB targeting mAbs. The neuropeptide NK-1900, for example, improved scopolamine-induced learning impairments and memory deficits in rats by i.v. administration of NK-1900-loaded polymersomes conjugated to an antitransferrin receptor mAb (OX-26) [12]. Previous studies by our group showed that polymersomes consisting of poly(dimethylsiloxane)-*b*-poly(2-methyloxazoline) (PDMS-*b*-PMOXA) modified with 83-14 mAb were taken up specifically by human brain capillary endothelial cells *in vitro* [13]. With K_D of 0.45 ± 0.10 nM, 83-14 mAb has a strong affinity to the α-subunit of the insulin receptor expressed on human brain capillary endothelial cells (hBMEC). Its binding to the HIR was shown to trigger receptor-mediated endocytosis *in vivo* and 83-14 mAb was shown to cross the primate BBB 10x more efficiently as compared to an antitransferrin receptor mAb [14, 15].

With respect to polymer-based NPs, however, the question arises if these particles can be safely degraded after delivering their drug payload, since accumulation and persistence within the target tissue are of potential safety concern. For example, PDMS-*b*-PMOXA vesicles used in our previous studies are characterized by a high chemical and mechanical stability [16]. Polyacrylamide-based nanocarriers used previously to implement drug targeting strategies could give rise to potential toxicity due to degradation products [17]. Polylactic acid-based NPs have been shown to be readily degradable but lactic acid, a major degradation product, can lead to acidification of the metabolizing cell and organ [18–20].

To address these potential issues, this study aimed to design and use PEG-*b*-PCL SNPs ([PP-SNP]) as a safe alternative to existing technologies. This polymer is already approved by regulatory authorities such as the US Food and Drug Administration (FDA) for tissue engineering and drug delivery. PEG-*b*-PCL is known to be biocompatible and biodegradable and was therefore used to implement an active targeting strategy to the brain [21]. 83-14 mAb was covalently conjugated to the surface of [PP-SNP] by a PEG-spaced heterobifunctional linker. Resulting [PP-SNP]-[mAb] was then analysed using an array of analytical methods (i.e., TEM, cryo-TEM, dynamic light scattering [DLS], pyrene encapsulation, and fluorescence correlation spectroscopy [FCS]). Interactions with eukaryotic cells and potential toxic effects were studied in a well-characterized *in vitro* BBB model (hCMEC/D3) and the human hepatocellular carcinoma cell line HepG2 [13, 22].

2. Materials and Methods

2.1. Materials. PEG-*b*-PCL (PCL average $M_n \approx 13\,000$, PEG average $M_n \approx 5000$, stored at 4°C under argon atmosphere, batch number. MKBR7365V), pyrene (≥99%), anhydrous tetrahydrofuran (THF; ≥99.9%), anhydrous dimethyl sulfoxide (DMSO; ≥99.9%), 2-iminothiolane hydrochloride (Traut's reagent; ≥98%), 1,1′-dioctadecyl-3,3,3′,3′-tetramethylindocarbocyanine perchlorate (DiI; ≥98%) gold(III) chloride trihydrate, sodium citrate dihydrate (≥99%), and anti-mouse IgG (whole molecule) gold antibody (5 nm colloidal gold) were purchased from Sigma-Aldrich (Schnelldorf, Germany). NH_2-PEG-*b*-PCL (PCL average $M_n \approx 15\,500$, PEG average $M_n \approx 5000$, batch number. P18343-NH2EGCL) was purchased from Polymer Source (Montreal, Canada). $SM(PEG)_{24}$ and DyLight 488 NHS ester were purchased from Thermo Fisher Scientific (Waltham, MA, USA). Thiazolyl Blue (MTT reagent; ≥98%) was purchased from Carl Roth GmbH (Karlsruhe, Germany). Amicon Ultra-4 centrifugal filter units (10 kDa NMWL, 30 kDa NMWL) were purchased from Merck Millipore (Darmstadt, Germany). The hybridoma cell line producing 83-14 mAb was kindly provided by Professor Ken Siddle (Department of Clinical Biochemistry, University of Cambridge, UK). Cell culture reagents and chemicals are listed below.

2.2. Preparation of [PP-SNP]. [PP-SNP] composed of a mixture of amphiphilic diblock copolymers (95% mol/mol PEG-*b*-PCL and 5% mol/mol NH_2-PEG-*b*-PCL) was prepared using the cosolvent method, also called the solvent displacement method [23]. In brief, the block copolymer (5.3 mg) was dissolved in THF (50 μL) and stirred at 700 rpm. Phosphate-buffered saline (PBS; 157 mM Na, 140 mM Cl) EDTA 5 mM, pH 7.4 (1 mL) was added dropwise under constant stirring. The mixture was stirred at room temperature (RT) overnight. THF was removed by two consecutive steps: THF was allowed to evaporate during overnight stirring [24]. Buffer was subsequently exchanged by gel filtration chromatography using Superose 6 Prep column eluting with PBS, pH 7.4 [25]. DiI-loaded [PP-SNP] ([PP-SNP-DiI]) was produced by adding 1 μg DiI per mg of PEG-*b*-PCL to THF and particles were produced using the same protocol as described above.

2.3. Fluorescent Labeling of 83-14 mAb. 83-14 mAb (1 mg/mL in PBS, pH 8.0) was incubated with a 5x molar excess of NHS ester functionalized DyLight 488 for 1 h at RT ([mAb-DL]). The sample was purified using an Amicon Ultra-4 centrifugal filter unit (MWCO 10 kDa).

2.4. Conjugation of 83-14 mAb to SNPs. A heterobifunctional linker ($SM(PEG)_{24}$) was used to conjugate 83-14 mAb or 83-14 mAb DL to [PP-SNP] giving rise to [PP-SNP]-[mAb], [PP-SNP-DiI]-[mAb], [PP-SNP-Au]-[mAb], or [PP-SNP]-[mAb-DL], respectively. SNPs were prepared as described above and incubated with a 20x molar excess of linker for 1 h at RT in PBS EDTA 5 mM, pH 7.0. Unbound linker was removed using an Amicon Ultra-4 centrifugal filter unit (MWCO 30 kDa). In parallel, a 2x molar excess of fluorescently labeled 83-14 mAb in sodium borate 0.1 M pH 8.5 was thiolated using Traut's reagent, that is, 100x molar excess of 2-iminothiolane. After incubation for 1 h at RT, thiolated 83-14 mAb was purified by using an Amicon Ultra-4 centrifugal filter unit (MWCO 10 kDa). SNPs and thiolated 83-14 mAb DL were mixed and incubated at RT overnight. Unbound 83-14 mAb was separated by gel filtration chromatography (Superose 6

Prep, PBS pH 7.4). For all experiments, modified SNPs were used immediately after preparation.

2.5. Gold-Nanohybrid SNP Formation. To visualize [PP-SNP] in TEM, gold-nanohybrids [PP-SNP-Au] were prepared as described recently [26]. In brief, 5.3 mg of PEG-*b*-PCL was dissolved in THF (50 μL) and stirred at 700 rpm. The AuR-solution (1 mM $HAuCl_4$, 4.1 mM citrate) was added dropwise under constant stirring. The mixture was heated to 70°C under constant agitation at 300 rpm on the thermomixer (Thermomixer Comfort; Eppendorf, Hamburg, Germany). Free gold NPs were separated by gel filtration chromatography (Superose 6 Prep) using PBS pH 7.4 as an eluent. Free gold particles did not elute during gel filtration chromatography. They had a high affinity for the stationary phase and were retained in the chromatography column [26]. [PP-SNP-Au] and [PP-SNP-Au]-[mAb] were collected after 8–12 min using a column volume of 30 mL and a flow rate of 1 mL/min.

2.6. Characterization of [PP-SNP]. Morphology and size distribution of [PP-SNP] were analysed using TEM, cryo-TEM, and DLS. For TEM analysis, 5 μL of nonconjugated and conjugated SNPs was mounted on a carbon-coated copper grid, negatively stained with 2% uranyl acetate solution, and dried overnight. Samples were visualized using a Philips Morgagni 268D transmission microscope. Mean SNP size was determined based on $n = 50$ particles. For cryo-TEM analysis, 4 μL of the polymer suspension was adsorbed onto glow-discharged holey carbon-coated grid (Quantifoil, Großlöbichau, Germany), blotted with Whatman filter paper, and vitrified into liquid ethane at −178°C using a vitrobot (FEI Company, Eindhoven, Netherlands). Frozen grids were transferred onto a Philips CM200-FEG electron microscope using a Gatan 626 cryoholder. Electron micrographs were recorded at an accelerating voltage of 200 kV and a nominal magnification of 50 000x, using a low-dose system (10 $e^-/Å^2$) and keeping the sample at −175°C. Defocus values were −4 μm. Micrographs were recorded at 4 K × 4 K CMOS camera (TVIPS, Gauting, Germany). DLS measurements were performed using a Delsa Nano C Particle Sizer (Beckman Coulter, Brea, CA, USA) operated in back scattering mode (165° angle).

2.7. Critical Aggregation Concentration (CAC). To assess the stability of [PP-SNP] upon dilution, the CAC of PEG-*b*-PCL was determined. Pyrene was used as a fluorescent probe as described previously [27, 28]. Pyrene in acetone (0.5 mL, 2.4×10^{-6} M) was mixed with 2 mL of Milli-Q water and 0.05, 0.5, 5, 50, or 500 μg/mL of PEG-*b*-PCL. The mixtures were heated to 60°C for 1 h and allowed to cool down to RT. After degasing with N_2, the fluorescence of pyrene was measured (Spectramax M2 plate reader, Molecular Devices, Sunnyvale, CA, USA; excitation: λ_{ex} 332 nm; emission: λ_{em1} 373 nm, λ_{em2} 384 nm). The ratio of $\lambda_{em2}/\lambda_{em1}$ was plotted against the logarithm of the PEG-*b*-PCL concentration to determine the CAC.

2.8. Density Measurements and Specific Volume Calculations. Density of particle suspension was measured at 20°C using an Anton Paar Density Meter DMA 4500 M (Anton Paar GmbH, Graz, Austria). The measured density (g/cm^3) of a suspension containing nanoparticles was used to calculate the apparent specific volume (cm^3/g) of the nanoparticles ($v_{\text{PP-SNP}}$) according to [29]

$$v_{\text{PP-SNP}} = \left(\frac{1}{c_{\text{polymer}}}\right)\left(\frac{1}{\rho_{\text{suspension}}}\right) - \left(\frac{1 - c_{\text{polymer}}}{c_{\text{polymer}}}\right)\left(\frac{1}{\rho_{\text{blank}}}\right), \quad (1)$$

where $\rho_{\text{suspension}}$ is the measured density of the suspension, ρ_{blank} is the measured density of the buffer, and c_{polymer} is the weight fraction of the polymer. The apparent volume (cm^3) of one polymer molecule in the assembled state was calculated according to

$$v_{\text{polymer}} \approx \frac{M_w \times v_{\text{PP-SNP}}}{N_A}, \quad (2)$$

where M_w is the molecular weight of the polymer and N_A is the Avogadro constant. The aggregation number (N_{agg}) was then calculated according to

$$N_{\text{agg}} \approx \frac{V_{\text{PP-SNP}}}{v_{\text{polymer}}} = \frac{(4/3) \times \pi \times (D/2)^3}{v_{\text{polymer}}}, \quad (3)$$

where v_{polymer} is the apparent volume of one polymer molecule and $V_{\text{PP-SNP}}$ is the volume of one solid-sphere nanoparticle ([PP-SNP]) and D is the nanoparticle diameter as determined by DLS or TEM measurements.

2.9. Gold Labeling of 83-14 mAb. To visualize conjugated 83-14 mAb, antibodies were stained using an anti-mouse IgG-gold antibody. In brief, 0.25 mg of [PP-SNP]-[mAb] was incubated with 50 μL of the anti-mouse IgG-gold antibody for 1 h at RT. Free anti-mouse IgG-gold antibodies were separated by gel filtration chromatography (Superose 6 prep) eluting with PBS pH 7.4. Samples were negatively stained as described above and were analysed by TEM. To exclude unspecific binding of the anti-mouse IgG-gold antibody, [PP-SNP] was stained using the same protocol.

2.10. Fluorescence Correlation Spectroscopy (FCS). Fluorescence correlation spectroscopy (FCS) was used to determine the number of fluorescently labeled 83-14 mAb per [PP-SNP]-[mAb-DL]. Measurements were performed with an inverted confocal fluorescence laser scanning microscope (Zeiss LSM 510-META/ConfoCor 2; Carl Zeiss AG, Oberkochen, Germany) equipped with an argon laser (488 nm) and a 40x water immersion objective lens (Zeiss C-Apochromat 40x, NA 1.2). 15 μL of sample was measured on a cover glass (Huber & Co AG, Reinach, Switzerland) at RT. Fluorescence intensity fluctuations were analysed in terms of an autocorrelation function. Autocorrelation curves were obtained by taking the average of 10 measurements over 30 s. Diffusion times for free DyLight 488 and DyLight 88-labeled antibodies were independently measured and fixed in the fitting procedure

in order to reduce the number of free fitting parameters. Molecular brightness measurements were used to calculate the number of fluorescently labeled antibodies per [PP-SNP]-[mAb-DL].

2.11. Cell Culture. Immortalized human brain capillary endothelial cells, hCMEC/D3 cells, were obtained under license from the Institut National de la Santé et de la Recherche Médicale, Paris, France. hCMEC/D3 cells were grown in culture flasks coated with 0.1 mg/mL rat tail collagen type I (BD Bioscience, San Jose, CA, USA) and cultured in endothelial cell basal medium (Provitro GmbH, Berlin, Germany) supplemented with 5% fetal bovine serum (FBS; Amimed BioConcept, Allschwil, Switzerland), 1 ng/mL basic fibroblast growth factor (PeproTech, Hamburg, Germany), 5 μg/mL ascorbic acid, 1.4 μM hydrocortisone (Sigma-Aldrich, Schnelldorf, Germany), 10 μL/mL chemically defined lipid concentrate (Gibco Life Technologies, Carlsbad, CA, US), 10 mM HEPES (Sigma-Aldrich, Schnelldorf, Germany), 2 mM GlutaMAX (Gibco Life Technologies, Carlsbad, CA, US), 100 U/mL penicillin, and 100 mg/mL streptomycin (Sigma-Aldrich, Schnelldorf, Germany). Only passages 29 to 35 were used for experiments. Human liver HepG2 cells were kindly provided by Professor Doctor Dietrich von Schweinitz (University Hospital of Basel, Basel, Switzerland). HepG2 cells were cultured in Dulbecco's modified eagle medium (DMEM; Sigma-Aldrich, Schnelldorf, Germany; glucose 4500 g/L) supplemented with 10% FBS, 100 U/mL penicillin, and 100 mg/mL streptomycin.

2.12. MTT Assay. Cell viability was determined using the MTT assay as described previously [22]. Toxicity of [PP-SNP] and [PP-SNP]-[mAb] was tested on the target cell line (hCMEC/D3). In addition, the well-characterized and frequently used human hepatocellular carcinoma cell line HepG2 was used to confirm cell viability results in another cell line and to rule out cell line specific effects. In brief, cells were seeded at a density of 2×10^4/well in a 96-well plate (TPP, Trasadingen, Switzerland) coated with collagen type I (10 μg/cm^2) or poly-D lysine (0.04 mg/mL), respectively. [PP-SNP] and [PP-SNP]-[mAb] were diluted with complete or serum-free culture medium to a final concentration of 0.01–1 mg/mL. PBS concentration was kept constant for all [PP-SNP] concentrations. Cells were washed twice with Dulbecco's phosphate-buffered saline (DPBS) and incubated with particle dilutions for 24 h in triplicate. Terfenadine (20 μM) was taken as positive controls. Cells were washed three times with DPBS and MTT working solution (100 μL, Thiazolyl Blue 5 mg/mL) was added. After 1.5–3 h, MTT working solution was aspirated and resulting formazan crystals were dissolved with DMSO (100 μL) protected from light for 15 min on an orbital shaker at RT. Absorption of dissolved formazan was measured at 570 nm and unspecific signals measured at 670 nm were subtracted (Spectramax M2 plate reader, Molecular Devices, Sunnyvale, CA, USA). Cell viability was expressed as percentage, whereas cell viability of untreated cells was defined as 100%. MTT assays were performed in triplicate and repeated three times. To determine statistical significance, one-way analysis of variance (ANOVA) followed by Tukey's *post hoc* test using OriginPro (Version 9.1.0, OriginLab Corporation, Northampton, MA, USA) was performed.

2.13. Flow Cytometry. To analyse uptake of [PP-SNP]-[mAb-DL] and [PP-SNP-DiI]-[mAb], flow cytometry was used. hCMEC/D3 cells were seeded at a density of 5×10^4 cells/cm^2 in a 12-well plate (TPP, Trasadingen, Switzerland). SNP formulations were diluted with culture medium to a final concentration of 0.1 mg/mL. Cells (80% confluency) were washed with DPBS and incubated with SNPs for 0.25, 0.5, 1, and 2 h. For competitive inhibition, cells were preincubated with a 100x excess of 83-14 mAb for 30 min at 37°C and washed twice with DPBS before incubating with SNPs. Washed cells were detached with 0.25% Trypsin-EDTA (Gibco Life Technologies, Carlsbad, CA, USA) for 3 min at 37°C and Trypsin-reaction was stopped by adding 1 mL of ice-cold DMEM supplemented with 10% FBS. The cell suspension of each well was collected, centrifuged at 200 g for 5 min (4°C), and washed three times with ice-cold DPBS. The pellets were resuspended in 500 μL of staining buffer (DPBS, 0.05% NaN_3, 1% FBS, EDTA 2.5 mM) and analysed by flow cytometry using a FACS Canto II flow cytometer (BD Bioscience, San Jose, CA, USA). Excitation wavelength was 488 nm and 561 nm. Cell doublets were excluded from analysis. The green fluorescence of DyLight 488 was detected using a 530/30 bandpass filter; the red fluorescence of DiI was detected using a 586/15 bandpass filter. Signals from 10 000–20 000 cells were normalised to max and analysed using FlowJo analysis software version V9/X (Tree-Star, Ashland, OR, USA). One-way analysis of variance (ANOVA) followed by Tukey's *post hoc* test using OriginPro (Version 9.1.0, OriginLab Corporation, Northampton, MA, USA) was performed to determine statistical significance.

2.14. Confocal Laser Scanning Microscopy (CLSM). Glass coverslips were placed in a 12-well plate and were coated with collagen (10 μg/cm^2). hCMEC/D3 cells were seeded at a density of 2.5×10^4 cells/cm^2 and allowed to adhere overnight. Level of confluency was 70–80%. Cells were washed with DPBS twice and incubated with [PP-SNP]-[mAb-DL], [PP-SNP-DiI], or [PP-SNP-DiI]-[mAb] (0.1 mg/mL) for 30 and 60 min at 37°C. Cell nuclei were stained by adding Hoechst 33342 dye (Eugene, OR, USA; 0.2 μg/mL) for 10 min. Cells were washed three times with ice-cold DPBS and fixed with freshly prepared paraformaldehyde (4%) for 15 min at 4°C. Paraformaldehyde was removed by washing three times with ice-cold DPBS; then cells were mounted with Prolong-Gold (Thermo Fisher Scientific, Waltham, MA, USA). Cells were analysed using an Olympus FV 1000 inverted laser scanning microscope and 40x (NA 1.30) and 60x (NA 1.40) oil immersion objectives (Olympus, Tokyo, Japan).

2.15. Transmission Electron Microscopy (TEM). Transwell polycarbonate membrane inserts (Corning, Baar, Switzerland; 0.4 μm pore size, 12 mm insert diameter) were coated with collagen type I (10 μg/cm^2) for 1 h at 37°C. Filters

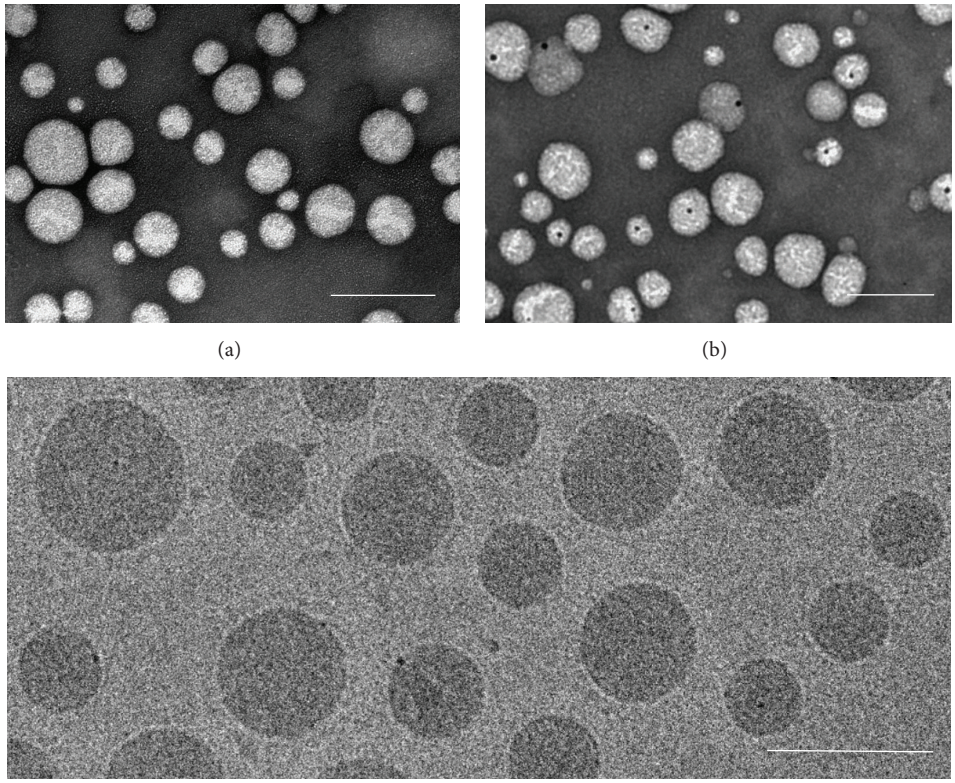

(a) (b)

(c)

Figure 1: Transmission electron microscope (TEM) images of PEG-*b*-PCL nanoparticles ([PP-SNP]). (a) TEM images [PP-SNP]. Size bar: 200 nm. (b) TEM image of gold-nanohybrid [PP-SNP] ([PP-SNP-Au]). Size bar: 200 nm. (c) Cryo-TEM images of [PP-SNP]. Size bar: 100 nm.

were washed twice with DPBS and hCMECM/D3 cells were seeded at a density of 5×10^4 cells/cm^2. Cells were grown to confluency for 8 days; medium was exchanged at days 4 and 7. At day 8, hCMEC/D3 cells were incubated with colloidal gold-loaded [PP-SNP-Au]-[mAb] at a final concentration of 0.1 mg/mL on the apical side for 0.25, 0.5, 1, 2, and 4 h. Cells were incubated with fixing medium (3% formaldehyde, 0.3% glutaraldehyde) at 4°C overnight. Cells were carefully rinsed three times with Hepes buffer (0.5 M, pH 7.0) and dehydrated using methanol. hCMEC/D3 cells were infiltrated with LR-Gold (PolyScience, Warrington, PA, USA) according to the manufacturer's instructions. The filter membrane was removed from the transwell insert using a scalpel. Membrane cuts were placed on a polymerized drop of resin in a plastic flat embedding mold and covered with a fresh resin. Polymerization was induced by UV-light at −10°C for 24 h. Sections of 70 nm were cut and collected on a carbon-coated Ni-grids and stained with uranyl acetate (2%) for 15 min and with lead citrate (Reynold's solution) for 2 min. Sections were analysed using a Philips CM 100 TEM.

3. Results

3.1. Characterization. TEM micrographs of [PP-SNP] showed spherical particles with a homogenous size distribution (Figure 1(a)). Mean diameter of $n = 50$ particles determined by TEM was 67 ± 15 nm. Size and size distribution of [PP-SNP] were confirmed by DLS. A mean hydrodynamic diameter of 78.2 ± 1.7 nm and a narrow size distribution (0.069 ± 0.021) were determined (Table 1). The zeta potential was −4.13 ± 0.24 (Table 1). In buffer (PBS, pH 7.4, room temperature), [PP-SNP] was stable for at least 2 months as shown by a constant particle size and a PDI below 0.2. To characterize the core structure of the NPs, cryo-TEM was performed. In cryo-TEM, a well-defined membrane can be observed for polymersomes, while no such structure is visible in micelles and solid-sphere NPs [30]. No membrane was observed in micrographs of [PP-SNP] as shown in Figure 1(c), indicating the solid-sphere structure of [PP-SNP]. Therefore, these particles were

Table 1: Comparison of nonconjugated PEG-*b*-PCL SNPs ([PP-SNP]) and targeted [PP-SNP]-[mAb]. [PP-SNP] and [PP-SNP]-[mAb] were analysed and the hydrodynamic diameter, polydispersity index (PDI), zeta potential, morphology, and the number of antibodies per NP (mAb/NP ratio) were compared ($n = 3$ experiments; values are means ± S.E.M).

	[PP-SNP]	[PP-SNP]-[mAb]
Hydrodynamic diameter (nm)	78.2 ± 1.7	79.9 ± 2.4
PDI	0.069 ± 0.021	0.079 ± 0.021
Zeta potential (mV)	−4.13 ± 0.24	2.43 ± 0.16
Morphology	Spherical	Spherical
mAb/NP ratio	—	5

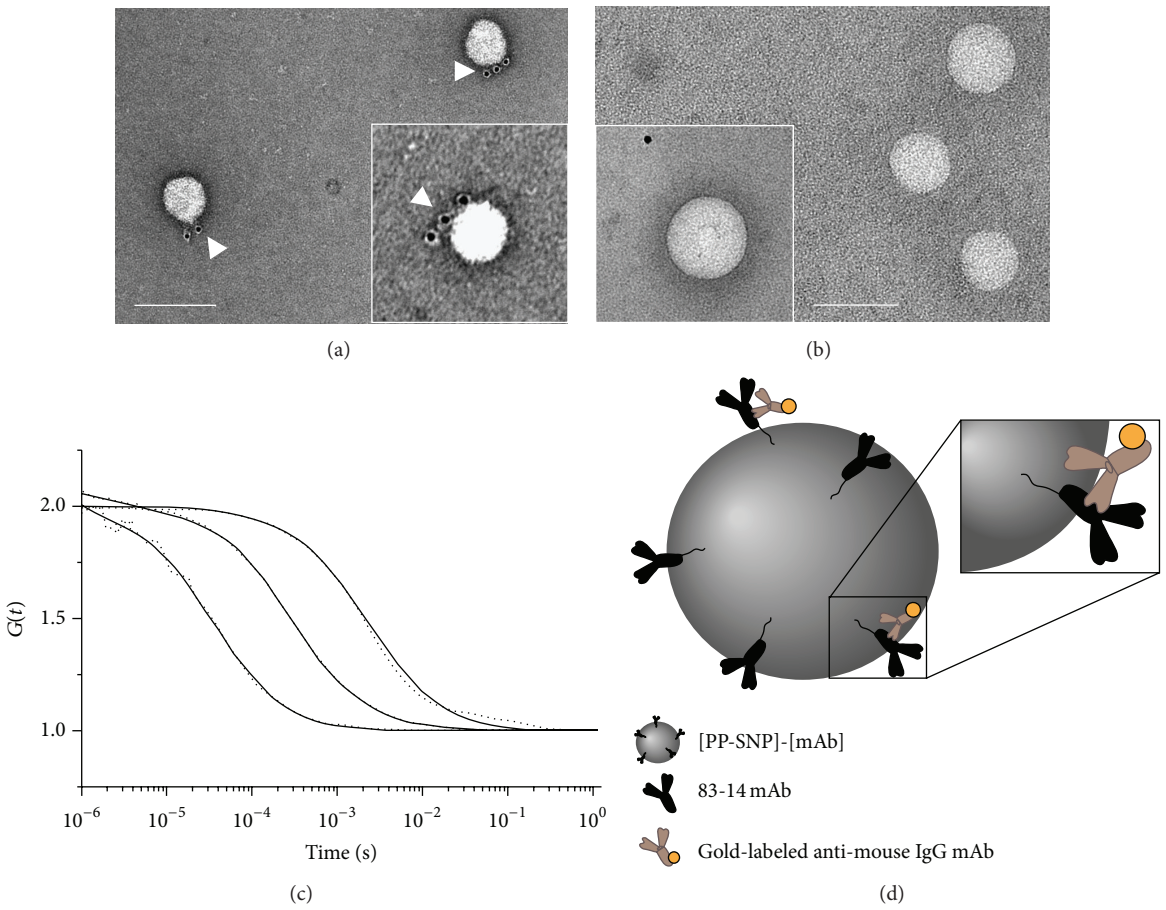

Figure 2: Determination of the mAb/NP ratio by transmission electron microsopy and fluorescence correlation spectroscopy. ((a) and (b)) Visualization of 83-14 mAb using a 5 nm colloidal gold-labeled anti-mouse IgG monoclonal antibody (white arrows). (a) PEG-*b*-PCL solid-sphere nanoparticles [PP-SNP] covalently conjugated to 83-14 mAb ([PP-SNP]-[mAb]). (b) Nonmodified [PP-SNP] after control incubation with gold-labeled anti-mouse IgG mAb (secondary mAb only). Size bar: 100 nm; insert: 2x magnification of a single NP and a noninteracting gold-labeled secondary antibody before purification. (c) FCS analysis of PEG-*b*-PCL SNPs conjugated to DyLight 488-labeled 83-14 mAb ([PP-SNP]-[mAb-DL]). Dotted line: free DyLight 488; dot-dashed line: DyLight 488-labeled 83-14 mAb; dashed line: [PP-SNP]-[mAb-DL]; solid lines: normalized autocorrelation curves. (d) Schematic drawing of [PP-SNP]-[mAb] incubated with colloidal gold-labeled anti-mouse IgG mAb.

classified as solid-sphere nanoparticles (SNPs). The CAC was determined using a hydrophobic fluorescent probe [27, 28]. By this technique, changes in fluorescence characteristics of fluorescent dyes, induced by their environment, are analysed. Thus, lipophilic dyes will be redistributed to the hydrophobic PCL-core of [PP-SNP] at concentrations above the CAC. The CAC of PEG-*b*-PCL determined by pyrene encapsulation during this study was 5 μg/mL (2.8×10^{-7} M). In this study, *in vitro* cell uptake experiments were always performed at 0.1 mg/mL, a concentration that is about 20 times higher than the determined CAC. The specific volume $v_{\text{PP-SNP}}$ of the [PP-SNP] suspension was determined to be 0.87 ± 0.01 cm^3/g.

3.2. Functionalization. To covalently conjugate 83-14 mAb to [PP-SNP], a PEG-spaced heterobifunctional linker was used. The linker was reactive towards primary amines (i.e., NH_2-PEG-*b*-PCL as a constituent of [PP-SNP]) and sulfhydryl groups (i.e., thiolated 83-14 mAb). FCS was used to quantify the number of fluorescently labeled antibodies per [PP-SNP]-[mAb-DL]. Figure 2(c) shows the normalized autocorrelation curves of free DyLight 488 dye, DyLight 488-labeled 83-14 mAb ([mAb-DL]), and [PP-SNP] conjugated to DyLight-labeled mAbs ([PP-SNP]-[mAb-DL]). Diffusion times for [mAb-DL] and [PP-SNP]-[mAb-DL] were 282 μs and 2594 μs. The increase in the diffusion times observed indicated the immobilization of [mAb-DL] on [PP-SNP]-[mAb-DL]. The mAb/NP ratio was determined by comparing the mean molecular brightness (CPM) of [PP-SNP]-[mAb-DL] (CPM = 85 kHz) to [mAb-DL] (CPM = 17 kHz). The CPM of [PP-SNP]-[mAb-DL] was 5x higher than the CPM of [mAb-DL]. Therefore, on average, 5 antibodies were conjugated to one [PP-SNP]-[mAb-DL]. Covalently attached 83-14 mAb to the surface of SNPs was furthermore visualised by TEM. Schematic drawing is shown in Figure 2(d). [PP-SNP]-[mAb] was incubated with a gold-labeled secondary mAb directed towards murine IgGs to visualize 83-14 mAb (Figure 2(a)). Gold particles were located in close proximity to the [PP-SNP]-[mAb] surface confirming 83-14 mAb presence

and accessibility. When nonfunctionalized [PP-SNP] was stained according to the same protocol, gold particles were not immobilized on SNP surface before (Figure 2(b) insert) and after purification using gel filtration chromatography (Figure 2(b)). This result indicates specific binding of the secondary mAb.

3.3. Toxicity. SNPs composed of the FDA-approved, biodegradable PEG-*b*-PCL show high biocompatibility [21, 31]. This is particularly important with respect to brain delivery of SNPs since accumulation of polymeric material could lead to toxic side effects within the CNS. To confirm these findings, hCMEC/D3 cells and a human hepatocellular carcinoma cell line (HepG2) were incubated with [PP-SNP] and [PP-SNP]-[mAb] (0.01–1 mg/mL) to analyse cell viability using the MTT assay. Even high polymer concentrations of up to 1 mg/mL caused only a slight decrease in cell viability. Uptake experiments were performed with 0.1 mg/mL PEG-*b*-PCL. This concentration does not show any significant cytotoxic effects on HepG2 and hCMEC/D3 cells.

3.4. Uptake. To study cellular uptake, hCMEC/D3 cells were incubated with [PP-SNP-DiI]-[mAb] or [PP-SNP-DiI] for 30 and 60 min and analysed using flow cytometry. Mean fluorescence intensity (MFI) increased in a time dependent manner (Figure 4). A representative flow cytometry graph is shown in Figure 5(b). For cells incubated with nonmodified [PP-SNP-DiI], increase in MFI of 7.7 ± 1.6 and 21.2 ± 4.3 was observed after 30 min and 1 h of incubation as compared to blank control cells. When cells were incubated with [PP-SNP-DiI]-[mAb], a significant increase in MFI was observed. A 2x increase in MFI was observed after 30 min (MFI = 16.3 ± 1.6) and 1 h (MFI = 38.9 ± 6.7) as compared to cells incubated with their nonmodified counterparts (Figure 4). [PP-SNP-DiI]-[mAb]-uptake could be inhibited competitively by preincubating the cells with an excess of free, unlabeled 83-14 mAb (MFI = 26.3 ± 4.8) as shown in Figures 4 and 5(b). To confirm these findings, the experiments were repeated using an alternative labeling method for the NPs. 83-14 mAb covalently labeled with DyLight 488 was conjugated to [PP-SNP] ([PP-SNP]-[mAb-DL]). Again, MFI decreased and was close to untreated control cells when cellular uptake was competitively inhibited (Figure 5(a)). In addition, SNP uptake by hCMEC/D3 cells was analysed using CLSM (Figure 5(c)). hCMEC/D3 cells were incubated with 0.1 mg/mL of [PP-SNP-DiI] or [PP-SNP-DiI]-[mAb] for 30 min. Distinct fluorescence signals (red dots) were observed close to the cell nuclei in the DiI-channel. Competitive inhibition reduced the [PP-SNP-DiI]-[mAb] signal. To study the intracellular localization of SNPs, gold-nanohybrids functionalized with 83-14 mAb ([PP-SNP-Au]-[mAb]) were prepared. Using such gold-nanohybrids, intracellular trafficking could be visualised by electron microscopy as a result of the high electron density of the Au-core whereas morphology, size, and PDI of [PP-SNP-Au] are similar to [PP-NP] (Figures 1(b) and 6(d)). Encapsulated gold NPs have a diameter of 14.1 ± 3.1 nm as shown previously [26]. Intracellular vesicles with [PP-SNP-Au]-[mAb] were observed after 15 min (Figures 6(a)–6(c)). After 60 min of incubation, [PP-SNP-Au]-[mAb] was detected in multivesicular bodies (MVBs; Figure 7).

4. Discussion

In this study, PEG-*b*-PCL diblock copolymer was used to produce a nanosized drug delivery system. SNPs were prepared using the cosolvent method at a final concentration of 5.3 mg/mL polymer. Particles assembled immediately after stirring at 700 rpm and adding PBS dropwise. This method is easy to handle, fast, and highly reproducible and uses no expensive or complex equipment. A fast preparation protocol is of huge advantage for different applications, for example, for scale-up or when radiolabeled NPs are prepared for pharmacokinetics studies. To target the NPs towards a specific tissue or cell type, ligands have to be attached to the NP surface. Different strategies can be used for such modifications. Since different classes of targeting moieties (e.g., mAbs, peptides, or small molecules) may require different conjugation strategies, a universal coupling tool is advantageous. Therefore, 5% mol/mol of amine-terminated PEG-*b*-PCL (NH_2-PEG-*b*-PCL) was used to covalently couple targeting moieties to [PP-SNP] by using the heterobifunctional linker $SM(PEG)_n$. $SM(PEG)_n$ contains an amine-reactive NHS ester functionality and maleimide that reacts to a metabolically stable thioether in the presence of sulfhydryl groups. A PEG-spacer of variable length links the two reactive groups. While a very low degree of functionalization was observed using $SM(PEG)_2$ with a spacer length of 17.6 Å, conjugation with 24 PEG-subunit long $SM(PEG)_{24}$ (spacer length: 95.2 Å) resulted in an increased mAb/NP ratio per [PP-SNP]-[mAb] using the same reaction conditions. Furthermore, PEG-spacers also can prevent the covalently attached mAb from being covered by particle-adsorbed biomolecules [32]. FCS was used to determine the mAb/NP ratio. On average, 5 molecules of fluorescently labeled 83-14 mAb were conjugated to the surface of one [PP-SNP]-[mAb-DL] (Figure 2(c)). FCS was used similarly in previous studies to determine the amount of fluorescently labeled molecules on SNPs [13, 33]. Radiolabeling, as typically used for the quantification of antibodies per NP, can be avoided by using FCS [34]. The number of targeting moieties on the NP surface influences the interaction with the target cell and can promote cellular uptake but may lead to increased clearance from the blood circulation [35]. In addition, a defined and narrow size distribution and the surface charge are important determinants for the fate of nanoparticles upon systemic exposure. NPs with a size below 6 nm can easily be excreted by renal filtration, while NPs with >300 nm in diameter or with a high surface charge will be recognized and removed by the reticuloendothelial system [36, 37]. Noncharged, pegylated NPs with a diameter below 200 nm show reduced protein opsonisation and remain in the systemic circulation for hours [38].

In cryo-TEM micrographs, no membrane was observed for [PP-SNP] indicating a solid-sphere structure of [PP-SNP] (Figure 1(c)). In comparison to low-molecular weight surfactants, SNPs show a low CAC, which is important for stability and drug retention. A high CAC can lead to a micelle collapse and subsequent burst release of the incorporated

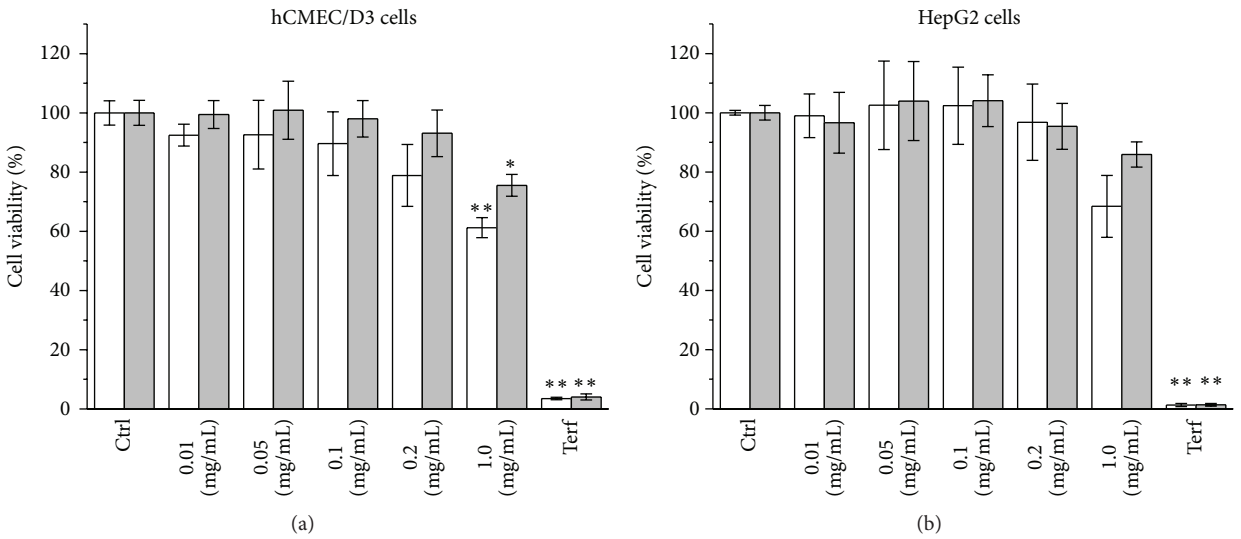

Figure 3: Cell viability of hCMEC/D3 and HepG2. hCMEC/D3 and HepG2 cells were incubated with 0.01–1.0 mg/mL PEG-*b*-PCL solid-sphere nanoparticles ([PP-SNP]) and 83-14 mAb modified [PP-SNP] ([PP-SNP]-[mAb]). Cell viability was analysed using the MTT assay 24 h after incubation. Cell viability is expressed as % viable cells compared to untreated control cells. Terfenadine (Terf) was used as positive control. White bars: [PP-SNP]-[mAb]; grey bars: [PP-SNP]. ANOVA and Tukey's *post hoc* means comparison was used to test for statistical significance ($n = 3$ experiments; $^{**}p < 0.05$; $^{*}p < 0.1$; S.E.M. is shown with error bars).

drug upon dilution in the blood compartment [10, 39]. Whereas typical low-molecular weight surfactants have CAC values in the range of 10^{-3}–10^{-4} M, CACs of diblock polymers can typically be found in range 10^{-6}–10^{-7} M. Additionally, the kinetic stability of the core structure of SNPs is high and thus the disassembly of SNPs after dilution below the CAC occurs slowly allowing an efficient retention of their drug payload [40]. The CAC of [PP-SNP] was determined using a fluorescent probe-based approach as described previously [28]. The CAC of PEG-*b*-PCL is 5 μg/mL (2.8×10^{-7} M), comparable to previously published data characterizing similar polymers [27].

The apparent specific volume $v_{\text{PP-SNP}}$ of the [PP-SNP] suspension was calculated from the measured density as described by Sommer et al. [29]. $v_{\text{PP-SNP}}$ was 0.87 ± 0.01 cm^3/g, which is close to the specific volume determined for micelles formed by the PEG-derived nonionic surfactant "Brij" [29]. Using this result, one can calculate the apparent volume of a single PEG-*b*-PCL polymer molecule (v_{polymer}) according to (2). In our experiment, v_{polymer} was 51 nm^3. The aggregation number (N_{agg}) of [PP-SNP] can then be estimated according to (3). A similar approach using apparent volumes to calculate aggregation numbers was proposed previously to determine N_{agg} of NPs consisting of a cell-penetrating peptide [41]. Since this calculation depends on the diameter of the particle, N_{agg} covers a range of ~2200 to ~10 000 for [PP-SNP] with diameters of 60 to 100 nm, respectively. These numbers are higher than results obtained by, for example, static light scattering (SLS) or fluorescent techniques where typical N_{agg} for diblock copolymer micelles are lower than 1000 [42, 43].

Among the broad range of polymer-based DDS, NPs composed of the FDA-approved, biodegradable PEG-*b*-PCL show high biocompatibility [21, 31, 44]. This is an important advantage regarding organ delivery of NPs since accumulation of polymeric material might lead to toxic side effects, for example, in the CNS. Because toxic effects of polymeric NPs on cells are driven not only by the polymeric material but also by many other characteristics including particle size, charge, or impurities, each NP formulation needs to be tested [45]. Toxicity of [PP-SNP] and [PP-SNP]-[mAb] on hCMEC/D3 cells was tested using the MTT assay. [PP-SNP] induced only a slight decrease in cell viability on hCMEC/D3 cells if incubated in concentrations up to 0.2 mg/mL (Figure 3). Cells incubated with [PP-SNP]-[mAb] showed as well a high cell viability. Even at high concentrations of 1 mg/mL, more than 60% of the incubated cells were viable. For cellular uptake experiments performed in this work, a concentration of 0.1 mg/mL was used. At this concentration the decrease in cell viability was negligible. The MTT assay was repeated with a second cell line to confirm the biocompatibility of the nanoparticles and to rule out cell line specific effects. The human hepatocellular carcinoma derived cell line HepG2 was used. Again, only a slight decrease in cell viability was observed (Figure 3). We conclude from these experiments that PEG-*b*-PCL SNPs are well tolerated within a typical dose range used in nanomedicine [22].

[PP-SNP-DiI]-[mAb] was taken up by hCMEC/D3 cells. These cells express similar HIR protein levels as freshly isolated hBMECs (1 fmol HIR/μg protein) and were therefore successfully used as an *in vitro* targeting model in previous studies [13, 46–48]. A time dependent increase in the fluorescence signal was observed (Figure 4). Conjugation with 83-14 mAb leads to an increase in MFI. Furthermore, uptake was specific and mediated by the 83-14 mAb since competition for the target receptor (HIR) with free mAb leads to a decrease of intracellular fluorescence (Figures 4

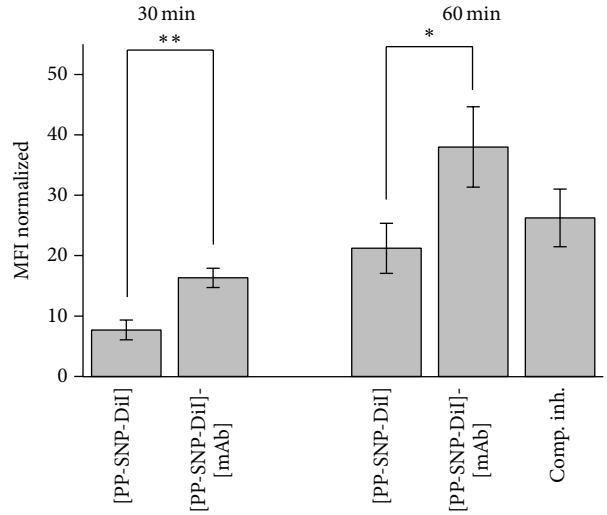

Figure 4: Uptake of PEG-*b*-PCL nanoparticles ([PP-SNP]) by hCMEC/D3 cells. Uptake of DiI-loaded PEG-*b*-PCL solid-sphere nanoparticles ([PP-SNP-DiI]) and 83-14 modified [PP-SNP-DiI] ([PP-SNP-DiI]-[mAb]) by hCMEC/D3 cells. Cells were incubated with SNPs for 30 min or 1 h and cellular uptake was analysed by flow cytometry. Mean fluorescence intensity (MFI) was normalized to untreated control cells. ANOVA and Tukey's *post hoc* means comparison was used to test for statistical significance ($n = 3$ experiments; $^{**}p < 0.05$; $^{*}p < 0.1$; S.E.M. is shown with error bars).

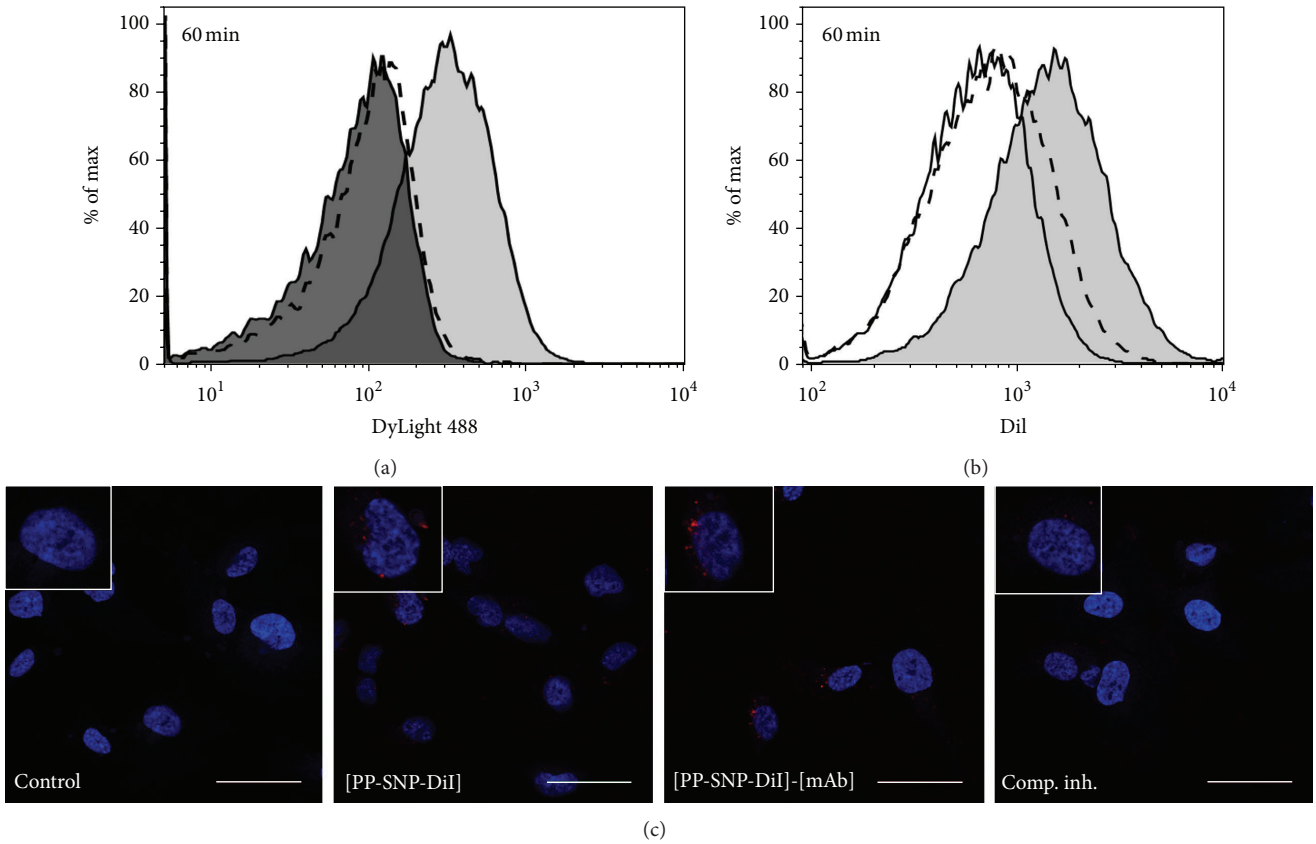

Figure 5: Cellular uptake of PEG-*b*-PCL nanoparticles ([PP-SNP]) analysed by flow cytometry and confocal laser scanning microscopy (CLSM). (a) Flow cytometry analysis of uptake of [PP-SNP] conjugated to DyLight 488-labeled 83-14 mAb ([PP-SNP]-[mAb-DL]) by hCMEC/D3 cells. Dark grey shaded: untreated cells; light grey shaded: cells incubated with [PP-SNP]-[mAb-DL] for 1 h; dashed line: cells incubated with [PP-SNP]-[mAb-DL] in the presence of a 100x excess of unlabeled 83-14 mAb. (b) Flow cytometry analysis of cellular uptake (hCMEC/D3) of DiI-loaded [PP-SNP] ([PP-SNP-DiI]) and 83-14 mAb modified [PP-SNP-DiI] ([PP-SNP-DiI]-[mAb]) after 1 h of incubation. Solid line: [PP-SNP-DiI]; dashed line: cells incubated with [PP-SNP-DiI]-[mAb] in the presence of a 100x excess of unlabeled 83-14 mAb; light grey shaded: [PP-SNP-DiI]-[mAb]. (c) Cellular uptake of [PP-SNP-DiI] and [PP-SNP-DiI]-[mAb] analysed by confocal laser scanning microscopy. Blue: nuclei stained with Hoechst 33342; red: [PP-SNP-DiI]-[mAb]. Size bar: 40 μm. Single-cell inserts: 2x magnification.

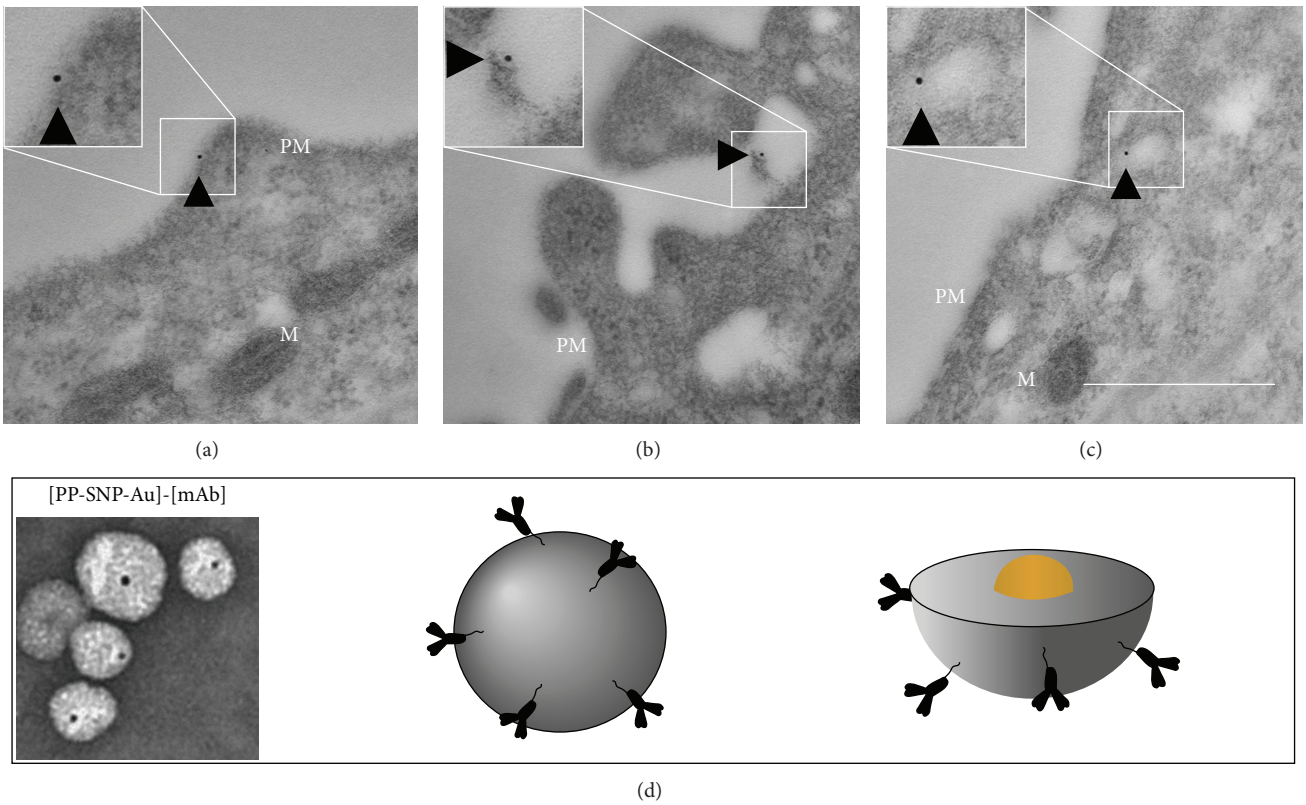

Figure 6: Uptake of gold-nanohybrid PEG-*b*-PCL nanoparticles conjugated to 83-14 mAb ([PP-SNP-Au]-[mAb]). ((a)–(c)) hCMEC/D3 cells were incubated with [PP-SNP-Au]-[mAb] for 15 min. Black arrows: gold particles; PM: plasma membrane; M: mitochondria. Size bar: 500 nm. (d) TEM image and schematic drawing of [PP-SNP-Au]-[mAb].

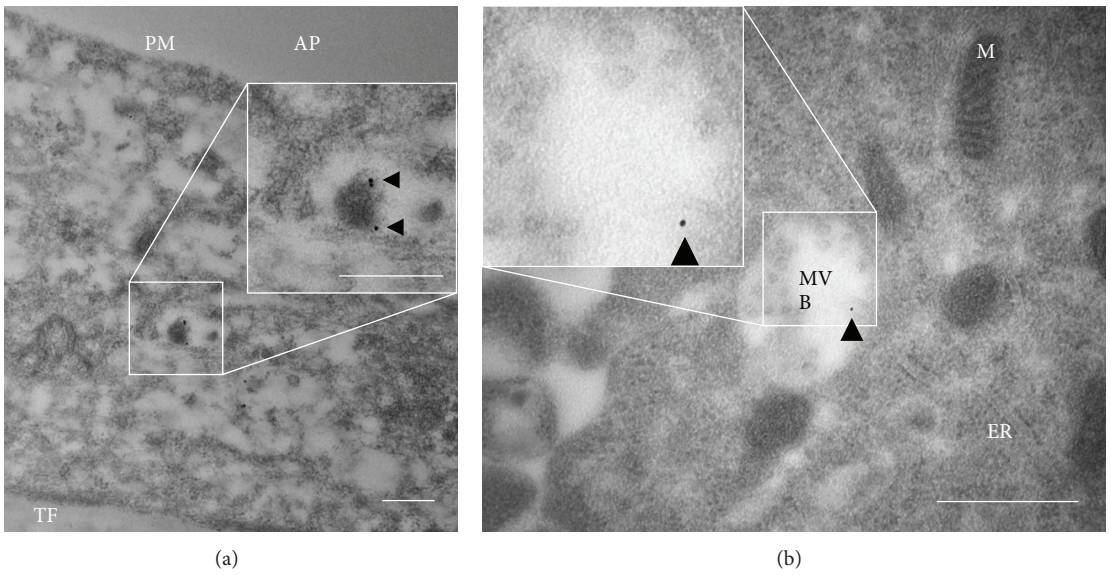

Figure 7: Intracellular localization of gold-nanohybrid PEG-*b*-PCL SNPs conjugated to 83-14 mAb ([PP-SNP-Au]-[mAb]). hCMEC/D3 cells were incubated with [PP-SNP-Au]-[mAb] for 60 min. (a) Cross section of a cell grown on a transwell insert. Size bar: 250 nm. Black arrows: gold particles. (b) [PP-SNP-Au]-[mAb] localized within a multivesicular body (MVB). Black arrows: gold particles; AP: apical compartment; PM: plasma membrane; TF: transwell filter membrane; M: mitochondria; ER: endoplasmic reticulum; MVB: multivesicular body. Size bar: 500 nm.

and 5). Immunoelectron transmission microscopy was used to study the subcellular localization of [PP-SNP-Au]-[mAb]. SNPs were visualized by a preembedding staining technique. To this end, a protocol to prepare gold-nanohybrids ([PP-SNP-Au]) was developed by our group [26]. This opens attractive possibilities to monitor intracellular trafficking of SNPs. hCMEC/D3 cells were grown on transwell inserts for 8 days as it was reported that hCMEC/D3 cells grown under these conditions show BBB characteristics and develop cell polarity [49]. This was furthermore demonstrated by their use for quantitative drug transport studies and qualitative analysis of albumin-gold-conjugates by TEM [50, 51]. [PP-SNP-Au]-[mAb] targeting the HIR was found in intracellular vesicles after 15 min of incubation at 37°C (Figure 6(c)). Accumulation in multivesicular bodies (MVBs) was detected after 60 min of incubation (Figure 7). Cellular uptake of gold-labeled insulin was studied previously using retinal vascular endothelial cells. It was shown that insulin was taken up fast and efficiently and accumulated in MVBs after 30 min of incubation [52]. However, cellular uptake of insulin seems to be faster and more efficient as compared to [PP-SNP-Au]-[mAb]. Similarly, previous studies using OX-26-immunoliposomes targeting the transferrin receptor showed that size is a crucial factor with respect to cellular uptake kinetics and efficiency. The permeability surface area product, a factor describing the BBB permeability, of the free OX-26 mAb was significantly higher as compared to the immunoliposomes *in vivo* [53]. In the present study, single colloidal gold particles were detected at all time-points, indicating that gold particles were taken up while incorporated into [PP-SNP-Au]-[mAb]. Free colloidal gold particles prepared without PEG-*b*-PCL agglomerated very fast and were found as clusters of particles when analysed by TEM [26]. To the best of our knowledge, this is the first study using gold-loaded targeted polymeric SNPs to visualize their uptake in a cell-based model. Further experiments such as quantitative *in vitro* transport studies and colocalization studies by fluorescent imaging, as performed previously, could help to identify the uptake mechanism of 83-14 modified SNPs [13, 54–56].

5. Conclusion

SNPs of the biodegradable diblock copolymer PEG-*b*-PCL were prepared and characterized *in vitro*. Our SNPs are characterized by a hydrodynamic diameter of 79.6 nm, a homogeneous size distribution, a slightly negative zeta potential, and a low CAC in the submicromolar range. In second step, [PP-SNP] was conjugated to anti-HIR mAb to enhance the cellular uptake by hCMEC/D3 cells. This resulted in targeted [PP-SNP]-[mAb] decorated with 5 molecules of mAb per SNP. [PP-SNP]-[mAb] was taken up by human BBB endothelial cells *in vitro* as shown by confocal microscopy and flow cytometry. Furthermore, the intracellular localization of gold-nanohybrids [PP-SNP-Au]-[mAb] in hCMEC/D3 cells grown on transwell inserts was analysed by TEM. Accumulation in multivesicular bodies of target cells was observed after 60 min of incubation. A similar behaviour was described for gold-labeled insulin [52]. Our *in vitro* data suggest that SNPs consisting of PEG-*b*-PCL are well tolerated. They are promising candidates for the implementation of a targeted drug delivery strategy. Further experiments will be needed to explore their potential in experimental animals.

Competing Interests

The authors report no conflicts of interest.

Acknowledgments

The authors wish to acknowledge Dr. Mohamed Chami and C-CINA (Center for Cellular Imaging and NanoAnalytics; Biozentrum, University of Basel) for acquiring cryo-TEM micrographs of [PP-SNP]; Dr. Timothy Sharpe (Head of Biophysics Facility, Biozentrum University of Basel) for his scientific advices; Dr. Susanne Schenk (Department of Pharmaceutical Sciences, University of Basel) for her scientific input during the project; and the Microscopy Center of the University of Basel for their support with electron microscopy. Cristina Prescianotto-Baschong received support from Grant 31003A-125423, awarded to Professor Dr. Martin Spiess (Biozentrum University of Basel) by the Swiss National Science Foundation.

References

[1] D. J. Begley, "Delivery of therapeutic agents to the central nervous system: the problems and the possibilities," *Pharmacology & Therapeutics*, vol. 104, no. 1, pp. 29–45, 2004.

[2] W. M. Pardridge, "Drug targeting to the brain," *Pharmaceutical Research*, vol. 24, no. 9, pp. 1733–1744, 2007.

[3] C.-T. Lu, Y.-Z. Zhao, H. L. Wong, J. Cai, L. Peng, and X.-Q. Tian, "Current approaches to enhance CNS delivery of drugs across the brain barriers," *International Journal of Nanomedicine*, vol. 9, no. 1, pp. 2241–2257, 2014.

[4] K. R. Duffy and W. M. Pardridge, "Blood-brain barrier transcytosis of insulin in developing rabbits," *Brain Research*, vol. 420, no. 1, pp. 32–38, 1987.

[5] W. M. Pardridge, J. Eisenberg, and J. Yang, "Human blood—brain barrier insulin receptor," *Journal of Neurochemistry*, vol. 44, no. 6, pp. 1771–1778, 1985.

[6] W. M. Pardridge, J. Eisenberg, and J. Yang, "Human blood-brain barrier transferrin receptor," *Metabolism*, vol. 36, no. 9, pp. 892–895, 1987.

[7] R. J. Boado, J. Z. Lu, E. K.-W. Hui, and W. M. Pardridge, "Insulin receptor antibody-sulfamidase fusion protein penetrates the primate blood-brain barrier and reduces glycosoaminoglycans in sanfilippo type A cells," *Molecular Pharmaceutics*, vol. 11, no. 8, pp. 2928–2934, 2014.

[8] A. Wicki, D. Witzigmann, V. Balasubramanian, and J. Huwyler, "Nanomedicine in cancer therapy: challenges, opportunities, and clinical applications," *Journal of Controlled Release*, vol. 200, pp. 138–157, 2015.

[9] W. Chen, F. Meng, R. Cheng, C. Deng, J. Feijen, and Z. Zhong, "Advanced drug and gene delivery systems based on functional biodegradable polycarbonates and copolymers," *Journal of Controlled Release*, vol. 190, pp. 398–414, 2014.

[10] G. Gaucher, M.-H. Dufresne, V. P. Sant, N. Kang, D. Maysinger, and J.-C. Leroux, "Block copolymer micelles: preparation,

characterization and application in drug delivery," *Journal of Controlled Release*, vol. 109, no. 1–3, pp. 169–188, 2005.

[11] V. P. Torchilin, "Polymer-coated long-circulating microparticulate pharmaceuticals," *Journal of Microencapsulation*, vol. 15, no. 1, pp. 1–19, 1998.

[12] Z. Pang, W. Lu, H. Gao et al., "Preparation and brain delivery property of biodegradable polymersomes conjugated with OX26," *Journal of Controlled Release*, vol. 128, no. 2, pp. 120–127, 2008.

[13] L.-H. Dieu, D. Wu, C. G. Palivan, V. Balasubramanian, and J. Huwyler, "Polymersomes conjugated to 83-14 monoclonal antibodies: *in vitro* targeting of brain capillary endothelial cells," *European Journal of Pharmaceutics and Biopharmaceutics*, vol. 88, no. 2, pp. 316–324, 2014.

[14] L. R. Walus, W. M. Pardridge, R. M. Starzyk, and P. M. Friden, "Enhanced uptake of rsCD4 across the rodent and primate blood-brain barrier after conjugation to anti-transferrin receptor antibodies," *Journal of Pharmacology and Experimental Therapeutics*, vol. 277, no. 2, pp. 1067–1075, 1996.

[15] D. Wu, J. Yang, and W. M. Pardridge, "Drug targeting of a peptide radiopharmaceutical through the primate blood-brain barrier in vivo with a monoclonal antibody to the human insulin receptor," *The Journal of Clinical Investigation*, vol. 100, no. 7, pp. 1804–1812, 1997.

[16] C. Nardin, M. Winterhalter, and W. Meier, "Giant free-standing ABA triblock copolymer membranes," *Langmuir*, vol. 16, no. 20, pp. 7708–7712, 2000.

[17] C.-Y. Huang and Y.-D. Lee, "Core-shell type of nanoparticles composed of poly[(n-butyl cyanoacrylate)-co-(2-octyl cyanoacrylate)] copolymers for drug delivery application: synthesis, characterization and *in vitro* degradation," *International Journal of Pharmaceutics*, vol. 325, no. 1-2, pp. 132–139, 2006.

[18] H. Liu, E. B. Slamovich, and T. J. Webster, "Less harmful acidic degradation of poly (lactic-co-glycolic acid) bone tissue engineering scaffolds through titania nanoparticle addition," *International Journal of Nanomedicine*, vol. 1, no. 4, pp. 541–545, 2006.

[19] G. C. Baltazar, S. Guha, W. Lu et al., "Acidic nanoparticles are trafficked to lysosomes and restore an acidic lysosomal pH and degradative function to compromised ARPE-19 cells," *PLoS ONE*, vol. 7, no. 12, Article ID e49635, 2012.

[20] F. Danhier, E. Ansorena, J. M. Silva, R. Coco, A. Le Breton, and V. Préat, "PLGA-based nanoparticles: an overview of biomedical applications," *Journal of Controlled Release*, vol. 161, no. 2, pp. 505–522, 2012.

[21] X. Wei, C. Gong, M. Gou et al., "Biodegradable poly(ε-caprolactone)-poly(ethylene glycol) copolymers as drug delivery system," *International Journal of Pharmaceutics*, vol. 381, no. 1, pp. 1–18, 2009.

[22] H. Kettiger, D. Sen Karaman, L. Schiesser, J. M. Rosenholm, and J. Huwyler, "Comparative safety evaluation of silica-based particles," *Toxicology in Vitro*, vol. 30, no. 1, pp. 355–363, 2015.

[23] R. Bleul, R. Thiermann, and M. Maskos, "Techniques to control polymersome size," *Macromolecules*, vol. 48, no. 20, pp. 7396–7409, 2015.

[24] X. Shuai, H. Ai, N. Nasongkla, S. Kim, and J. Gao, "Micellar carriers based on block copolymers of poly(ε-caprolactone) and poly(ethylene glycol) for doxorubicin delivery," *Journal of Controlled Release*, vol. 98, no. 3, pp. 415–426, 2004.

[25] I. Kim, S. A. Mckenna, E. V. Puglisi, and J. D. Puglisi, "Rapid purification of RNAs using fast performance liquid chromatography (FPLC)," *RNA*, vol. 13, no. 2, pp. 289–294, 2007.

[26] D. Witzigmann, S. Sieber, F. Porta et al., "Formation of lipid and polymer based gold nanohybrids using a nanoreactor approach," *RSC Advances*, vol. 5, no. 91, pp. 74320–74328, 2015.

[27] H. M. Aliabadi, A. Mahmud, A. D. Sharifabadi, and A. Lavasanifar, "Micelles of methoxy poly(ethylene oxide)-*b*-poly(ε-caprolactone) as vehicles for the solubilization and controlled delivery of cyclosporine A," *Journal of Controlled Release*, vol. 104, no. 2, pp. 301–311, 2005.

[28] E. D. Goddard, N. J. Turro, P. L. Kuo, and K. P. Ananthapadmanabhan, "Fluorescence probes for critical micelle concentration determination," *Langmuir*, vol. 1, no. 3, pp. 352–355, 1985.

[29] C. Sommer, J. S. Pedersen, and P. C. Stein, "Apparent specific volume measurements of poly(ethylene oxide), poly(butylene oxide), poly(propylene oxide), and octadecyl chains in the micellar state as a function of temperature," *Journal of Physical Chemistry B*, vol. 108, no. 20, pp. 6242–6249, 2004.

[30] S. A. Meeuwissen, S. M. C. Bruekers, Y. Chen, D. J. Pochan, and J. C. M. van Hest, "Spontaneous shape changes in polymersomes via polymer/polymer segregation," *Polymer Chemistry*, vol. 5, no. 2, pp. 489–501, 2014.

[31] T. Ameller, V. Marsaud, P. Legrand, R. Gref, and J.-M. Renoir, "Pure antiestrogen RU 58668—loaded nanospheres: morphology, cell activity and toxicity studies," *European Journal of Pharmaceutical Sciences*, vol. 21, no. 2-3, pp. 361–370, 2004.

[32] E. Mahon, A. Salvati, F. Baldelli Bombelli, I. Lynch, and K. A. Dawson, "Designing the nanoparticle-biomolecule interface for 'targeting and therapeutic delivery'," *Journal of Controlled Release*, vol. 161, no. 2, pp. 164–174, 2012.

[33] T. Einfalt, R. Goers, I. A. Dinu et al., "Stimuli-triggered activity of nanoreactors by biomimetic engineering polymer membranes," *Nano Letters*, vol. 15, no. 11, pp. 7596–7603, 2015.

[34] E. M. Cornford, S. Hyman, M. E. Cornford et al., "Non-invasive gene targeting to the fetal brain after intravenous administration and transplacental transfer of plasmid DNA using PEGylated immunoliposomes," *Journal of Drug Targeting*, vol. 24, no. 1, pp. 58–67, 2015.

[35] J. Huwyler, D. Wu, and W. M. Pardridge, "Brain drug delivery of small molecules using immunoliposomes," *Proceedings of the National Academy of Sciences of the United States of America*, vol. 93, no. 24, pp. 14164–14169, 1996.

[36] M. Hamidi, A. Azadi, and P. Rafiei, "Pharmacokinetic consequences of pegylation," *Drug Delivery*, vol. 13, no. 6, pp. 399–409, 2006.

[37] H. Kobayashi, B. Turkbey, R. Watanabe, and P. L. Choyke, "Cancer drug delivery: considerations in the rational design of nanosized bioconjugates," *Bioconjugate Chemistry*, vol. 25, no. 12, pp. 2093–2100, 2014.

[38] F. Alexis, E. Pridgen, L. K. Molnar, and O. C. Farokhzad, "Factors affecting the clearance and biodistribution of polymeric nanoparticles," *Molecular Pharmaceutics*, vol. 5, no. 4, pp. 505–515, 2008.

[39] V. P. Torchilin, "Structure and design of polymeric surfactant-based drug delivery systems," *Journal of Controlled Release*, vol. 73, no. 2-3, pp. 137–172, 2001.

[40] W. Xu, P. Ling, and T. Zhang, "Polymeric micelles, a promising drug delivery system to enhance bioavailability of poorly water-soluble drugs," *Journal of Drug Delivery*, vol. 2013, Article ID 340315, 15 pages, 2013.

[41] G. Québatte, E. Kitas, and J. Seelig, "RiDOM, a cell-penetrating peptide. Interaction with DNA and heparan sulfate," *Journal of Physical Chemistry B*, vol. 117, no. 37, pp. 10807–10817, 2013.

[42] X. Ye, J. Fei, K. Xu, and R. Bai, "Effect of polystyrene-*b*-poly(ethylene oxide) on self-assembly of polystyrene-*b*-poly(*N*-isopropylacrylamide) in aqueous solution," *Journal of Polymer Science Part B: Polymer Physics*, vol. 48, no. 11, pp. 1168–1174, 2010.

[43] L. Yang, X. Qi, P. Liu, A. El Ghzaoui, and S. Li, "Aggregation behavior of self-assembling polylactide/poly(ethylene glycol) micelles for sustained drug delivery," *International Journal of Pharmaceutics*, vol. 394, no. 1-2, pp. 43–49, 2010.

[44] S. Li, H. Garreau, B. Pauvert, J. McGrath, A. Toniolo, and M. Vert, "Enzymatic degradation of block copolymerase prepared from ε-caprolactone and poly(ethylene glycol)," *Biomacromolecules*, vol. 3, no. 3, pp. 525–530, 2002.

[45] L. Shang, K. Nienhaus, and G. U. Nienhaus, "Engineered nanoparticles interacting with cells: size matters," *Journal of Nanobiotechnology*, vol. 12, article 5, 2014.

[46] S. Ohtsuki, C. Ikeda, Y. Uchida et al., "Quantitative targeted absolute proteomic analysis of transporters, receptors and junction proteins for validation of human cerebral microvascular endothelial cell line hCMEC/D3 as a human blood-brain barrier model," *Molecular Pharmaceutics*, vol. 10, no. 1, pp. 289–296, 2013.

[47] Y. Uchida, S. Ohtsuki, Y. Katsukura et al., "Quantitative targeted absolute proteomics of human blood-brain barrier transporters and receptors," *Journal of Neurochemistry*, vol. 117, no. 2, pp. 333–345, 2011.

[48] D. Chirio, M. Gallarate, E. Peira et al., "Positive-charged solid lipid nanoparticles as paclitaxel drug delivery system in glioblastoma treatment," *European Journal of Pharmaceutics and Biopharmaceutics*, vol. 88, no. 3, pp. 746–758, 2014.

[49] B. B. Weksler, "Blood-brain barrier-specific properties of a human adult brain endothelial cell line," *The FASEB Journal*, vol. 19, no. 13, pp. 1872–1874, 2005.

[50] L. D. Simmler, T. A. Buser, M. Donzelli et al., "Pharmacological characterization of designer cathinones *in vitro*," *British Journal of Pharmacology*, vol. 168, no. 2, pp. 458–470, 2013.

[51] D. Ye, K. A. Dawson, and I. Lynch, "A TEM protocol for quality assurance of in vitro cellular barrier models and its application to the assessment of nanoparticle transport mechanisms across barriers," *The Analyst*, vol. 140, no. 1, pp. 83–97, 2015.

[52] A. W. Stitt, H. R. Anderson, T. A. Gardiner, J. R. Bailie, and D. B. Archer, "Receptor-mediated endocytosis and intracellular trafficking of insulin and low-density lipoprotein by retinal vascular endothelial cells," *Investigative Ophthalmology and Visual Science*, vol. 35, no. 9, pp. 3384–3392, 1994.

[53] A. Cerletti, J. Drewe, G. Fricker, A. N. Eberle, and J. Huwyler, "Endocytosis and transcytosis of an immunoliposome-based brain drug delivery system," *Journal of Drug Targeting*, vol. 8, no. 6, pp. 435–446, 2000.

[54] A. Grover, A. Hirani, Y. Pathak, and V. Sutariya, "Brain-targeted delivery of docetaxel by glutathione-coated nanoparticles for brain cancer," *Ageing International*, vol. 15, no. 6, pp. 1562–1568, 2014.

[55] A. R. Neves, J. F. Queiroz, B. Weksler, I. A. Romero, P. Couraud, and S. Reis, "Solid lipid nanoparticles as a vehicle for brain-targeted drug delivery: two new strategies of functionalization with apolipoprotein E," *Nanotechnology*, vol. 26, no. 49, Article ID 495103, 2015.

[56] X. Tian, S. Nyberg, P. S. Sharp et al., "LRP-1-mediated intracellular antibody delivery to the Central Nervous System," *Scientific Reports*, vol. 5, Article ID 11990, 2015.